Drug adaptation influences cardiotoxicity caused by tyrosine kinase inhibitors in iPSC-derived human cardiomyocytes

Huan Wang[1,2], Robert P. Sheehan[1,2], Adam C. Palmer[1,2], Robert A. Everley[1], Sarah A. Boswell[1,2], Noga Ron-Harel[3], Kristina M. Holton[4], Connor A. Jacobson[1], Alison Erickson[3], Laura Maliszewski[1,2], Marcia C. Haigis[3], Peter K. Sorger[1,2,*]

[1] Laboratory of Systems Pharmacology; Harvard Program in Therapeutic Science; Harvard Medical School; Boston, Massachusetts 02115, USA

[1] HMS LINCS Center, Harvard Medical School; Boston, Massachusetts 02115, USA

[2] Department of Systems Biology; Harvard Medical School; Boston, Massachusetts 02115, USA

[3] Department of Cell Biology; Harvard Medical School; Boston, Massachusetts 02115, USA

[4] Research Computing; Harvard Medical School; Boston, Massachusetts 02115, USA

*Corresponding author: Peter K. Sorger, Warren Alpert 444, 200 Longwood Avenue, Boston, Massachusetts 02115, peter_sorger@hms.harvard.edu, phone (617) 432-6901, fax (617) 432-6990

KEYWORDS: drug adaptation, tyrosine kinase inhibitor, human induced pluripotent stem cell-derived cardiomyocyte, cardiotoxicity, aerobic glycolysis, mitochondrial respiration, transcriptomics, Tandem Mass Tag Mass Spectrometry, high-content imaging.

SUMMARY

Cardiotoxicity induced by anti-cancer drugs is of increasing concern as the durability of therapeutic responses increases. The molecular basis of cardiotoxicity remains poorly understood, particularly when due to drug classes that do not inhibit the hERG potassium channel or cause the arrhythmias associated with long QT syndrome. This paper describes systematic molecular profiling of one such class of drugs, tyrosine kinase inhibitors (TKIs), which are widely used to treat solid tumors. Human cardiomyocytes differentiated from induced pluripotent stem cells (hiPSC-CMs) were exposed to one of four TKIs (Sunitinib, Sorafenib, Lapatinib and Erlotinib) observed to cause different levels of human cardiotoxicity and profiled by RNA sequencing (RNA-Seq) and mass spectroscopy-based proteomic analysis. We find that TKIs have diverse effects on hiPSC-CMs but genes involved in cardiac metabolism are particularly sensitive. In the case of Sorafenib, many genes involved in oxidative phosphorylation are down regulated resulting in a profound defect in mitochondrial metabolism. Cells adapt to this by upregulating aerobic glycolysis. Metabolic remodeling makes cells less acutely sensitive to Sorafenib and the effect is reversible upon drug withdrawal. Thus, the response of cardiomyocytes to Sorafenib is characterized by adaptive drug resistance previously described in tumor cells.

INTRODUCTION

As therapeutic responses to "targeted" anti-cancer drugs become increasingly sustained, drug-induced cardiotoxicity is a growing concern. Cardiotoxicity is observed in the use of a wide range of drugs, including tyrosine kinase inhibitors (Chu et al., 2007), immune checkpoint inhibitors (Johnson et al., 2016; Moslehi et al., 2018), nonsteroidal anti-inflammatory drugs (Bresalier et al., 2005) and proteasome inhibitors (Waxman et al., 2018). In patients, exposure to these drugs induces cardiotoxicity as defined by one or more of the following adverse effects: hypertension, arrhythmia, decreased left ventricular ejection fraction (LVEF), myocarditis, cardiac ischemia and cardiac failure (Magdy et al., 2018). A dramatic example involving chemotherapy is provided by pediatric patients treated with anthracyclines plus radiation. Such patients have a 7-fold higher risk of death due to cardiovascular damage than age-matched controls. In general, cardio-protective measures, such as drug holidays, dose reduction, and/or administration of β-adrenergic receptor or angiotensin-converting-enzyme (ACE) inhibitors are indicated following a decline in LVEF of greater than 10% (or if the absolute value is < 53% (Gavila et al., 2017)). However, treatment for drug-induced cardiotoxicity is limited: beta blockers and ACE inhibitors relieve the physiological symptoms of adverse cardiac events but do not alter the molecular processes responsible for cardiotoxicity or the resulting tissue damage.

The two forms of drug-induced cardiotoxicity best understood at a molecular level are exposure to anthracycline and drug-induced arrhythmias. The cumulative dose of anthracyclines is a strong predictor of risk for congestive heart failure (Von Hoff et al., 1979) and the anthracycline doxorubicin is known to inhibit topoisomerase, causing cardiotoxicity through DNA double-strand breaks (Zhang et al., 2012). Drug induced arrhythmias are often caused by disruption of the hERG potassium channel (the product of the KCNH2 gene), which controls cardiac repolarization (Roden, 2004; Vandenberg et al., 2012). The resultant long QT syndrome can be acutely life-threatening, making hERG an important anti-target for drug discovery.

Tyrosine kinase inhibitors (TKIs) are prototypical targeted anti-cancer therapies associated with varying degrees of cardiotoxicity that do not involve long QT syndrome or DNA damage. Both relatively selective and non-selective TKIs are associated with cardiotoxicity, and the number of kinases targeted by each drug is not obviously related to the magnitude of adverse effect (Moslehi and Deininger, 2015; Orphanos et al., 2009).

Among the drugs studied in this paper, Sunitinib (Suntent®) is most often associated with clinically detectable cardiotoxicity, including hypertension (8-47% occurrence among patients undergoing clinical trials), symptomatic depression of LVEF (9-28% in trials), and congestive heart failure (up to 8% in trials) (Chu et al., 2007; Motzer et al., 2007; Narayan et al., 2017). Sorafenib (Nexavar®) commonly causes hypertension (8-40% in trials) and less frequently cardiac ischemia (2-3% in trials) (Bhargava, 2009; Escudier et al., 2007). Cardiomyopathies induced by Sunitinib and Sorafenib arise after some time on drug (typically months) and are reversible following drug discontinuation (Francis et al., 2010; Schmidinger et al., 2008; Uraizee et al., 2011). In contrast, Lapatinib (Tykerb®)-associated cardiotoxicity is sporadic, less severe when it occurs, and is most often associated with asymptomatic decreases in LVEF (Dogan et al., 2012; Geyer et al., 2006; Perez et al., 2008). Erlotinib (Tarceva®) is very rarely associated with cardiac side-effects (Orphanos et al., 2009) and was included in our study as a bioactive, cardiotoxicity-negative control.

Previous *in vitro* and *in vivo* studies have established that TKIs can cause cardiotoxicity and hypertension through both on-target and off-target effects (Chen et al., 2008). Sunitinib and Sorafenib inhibit multiple receptor tyrosine kinases (RTKs) including VEGF Receptor (VEGFR) which is a known cause of hypertension (Schmidinger et al., 2008) albeit one that can usually be managed clinically (Robinson et al., 2010). Sunitinib has also been shown to induce cardiomyocyte apoptosis via inhibition of AMPK phosphorylation, an off-target effect (Kerkela et al., 2009). In addition, cardiomyocyte development and survival is dependent on many of the pathways inhibited by TKIs (e.g. PDGFRβ, VEGFR2, RAF1, etc.) although evidence that this is involved in toxicity remains limited (Force et al., 2007; Kerkela et al., 2006). The impact of duration of drug exposure is also unknown. In cultured cells, the acute and long-term effects of drugs often differ, with the former reflecting direct target inhibition and the latter drug-induced adaptation. In cancer cells, adaptive responses can result in drug tolerance (Sun et al., 2014) but whether this occurs in cardiomyocytes is unknown.

In this study, we profiled phenotypic and molecular responses to four widely used TKIs (Sunitinib, Sorafenib, Lapatinib and Erlotinib) in human induced pluripotent stem cell-derived cardiac myocytes (hiPSC-CMs) at varying drug doses and times of exposure. hiPSC-CMs are an increasingly popular culture system in which to study cardiac biology because they are readily available, genetically well-defined, and more

representative of human biology than conventional immortalized cell lines or rodent cardiomyocytes; hiPSC-CMs are, however, less mature than fully-differentiated human cardiomyocytes (Burridge et al., 2016; Sharma et al., 2017). Systematic profiling of hiPSC-CMs was initiated with three goals. First, it sought to establish the repeatability of molecular measurements across different batches of differentiated hiPSCs. Second, it sought to aquire matched proteomic and transcriptomic datasets for four TKIs across a range of drug doses and exposure times and determine how overall exposure relates to these variables. Third, it aimed to functionally investigate one adverse phenotype as a demonstration of the utility of the overall dataset for elucidating the mechanisms of cardiotoxicity. For the four TKIs studied, RNA-Seq and mass spec-based proteomics in hiPSC-CMs reveals widespread changes in cardiac metabolism and disruption of sarcomere proteins involved in contraction. The extent to which these processes were affected correlated with clinical cardiotoxicity across the four drugs tested. Metabolic reprograming was particularly apparent, and had the properties of an adaptive drug response.

RESULTS

Phenotypic responses to four TKIs in human iPSC-derived cardiomyocytes

Cor.4U hiPSC-CMs were obtained from the manufacturer (Axiogenesis; now Ncardia). The cells underwent directed differentiated from iPSCs created from a human female to cardiac myocytes. We plated Cor.4U cells in the vendor-specified growth medium containing 10% FBS for three days, switched them to minimal medium with 1% FBS and then added TKIs; cells were refed periodically and samples withdrawn for analysis (Fig. 1A). The differentiation of iPSC-CMs is known to be heterogeneous and cultures contain cells at different developmental stages (Karakikes et al., 2015). We assayed the maturity of Cor.4U hiPSC-CM cultures by immunofluorescence microscopy using two sarcomeric proteins: α-actinin and the cardiac isoform of Troponin T. Over 90% of Cor.4U cells stained positive for α-actinin and Troponin T two days after plating and both proteins were found in regular and alternating striations in the sarcomeres characteristic of functional cardiomyocytes (Fig. 1B and Supplementary Fig. 1); the remaining ~10% of cells appeared to be less fully differentiated cardiac progenitors. Cells with well-developed sarcomeres exhibited spontaneous contraction and calcium pulsing, which is typical of CMs in culture (Blinova et al., 2017).

The dose and time of TKI exposure needed to generate biologically meaningful data is not self-evident: cells in culture are sufficiently different from cells *in vivo* that the clinical maximum plasma concentration (C_{max}) is only a rough guide. C_{max} values for the four TKIs analyzed in this paper (Supplementary Table 1) are reported to range from 0.03 to 18 µM with considerable variability, which likely arises from inter-individual differences in adsorption, distribution, metabolism, and excretion (ADME; Supplementary Table 2). We therefore took an empirical approach using two phenotypic assays. Changes in cellular ATP levels as a function of drug dose and time were measured using the Celltiter-Glo® assay (which is often considered a proxy for cell viability) and mitochondrial membrane potential was measured using TMRE (Tetramethylrhodamine ethyl ester perchlorate) followed by fluorescence imaging. Cor.4U cells were exposed to each TKI at 1 of 8 drug doses ranging from 0.01 to 10 µM separated by half-log (~3 fold) steps; the time of exposure ranged from 6 hr to 1, 3, 5 or 7 days. For each drug, a dose range was chosen that lowered mitochondrial membrane potential but did not induce cell death (as measured by a reduction in cell number). We found that Lapatinib, Sorafenib, and Sunitinib induced death of Cor.4U cells at doses > 3 µM and long exposure times (over 5 days) but that mitochondrial membrane potential was reduced at lower doses. Erlotonib had little effect on mitochondrial membrane potential or cell viability under any condition tested. These data demonstrate the existence of a fairly wide exposure window in which TKIs induce a strong phenotype but cells remain viable and can therefore be subjected to molecular profiling. In addition, we found that the rank order of toxicity for the four TKIs on hiPSC-CMs was the same as previously reported for cardiotoxicity in human patients.

Changes in RNA expression induced by exposure of hiPSC-CMs to TKIs

To identify gene expression changes associated with TKI exposure, we systematically varied dose and time centered on the active concentration identified by measurement of mitochondrial membrane potential in Figure 1. The resulting cruciform design of seven conditions (including t=0) covered dose and time with a minimum number of samples. Cells were exposed to one of four TKIs at 3 µM for 6, 24, 72 or 168 hr and also at 1 µM and 10 µM drug for 24 hr (Fig. 2A). Each condition was assayed in biological triplicate, yielding 18 samples per drug or 84 overall, including DMSO-treated controls (available in GEO as GSE114686). Performing

a molecular profiling experiment at this scale requires use of multiple lots of Cor.4U cells; in our case, one lot per replicate.

Sequencing data were normalized for the time in culture by calculating expression fold changes relative to time-matched vehicle-only controls. In control cells, ~12,000 coding transcripts were detected; Pearson correlation coefficients for replicate assays from cells exposed to 10 μM Sorafenib or vehicle-alone for 24 hr were 0.96-0.99, demonstrating good reproducibility across batches of cells (Supplementary Fig. 2A). In the absence of TKI exposure, ~400-500 genes changed 1.5-fold or more in expression (FDR $\leq$ 0.05) over a period of seven days. Genes corresponding to the GO term "cell cycle" were the most frequently down-regulated (Supplementary Fig. 2B). Imaging showed that about 10% of the cells in the culture lacked regularly striated sarcomeres and appeared to be undifferentiated cardiac fibroblasts; it is likely that downregulation of cell-cycle associated genes arises from drug-induced arrest of a minor subpopulation of dividing iPSCs and fibroblasts (or perhaps, acquisition of more differentiated post-mitotic phenotype by these cells).

When all of the gene expression fold-change data were combined and principal component analysis (PCA) performed, the first two principal components (PC1 and PC2) explained ~80% of variance; this represents excellent performance for PCA (Fig. 2B). By rotating the axes of the PCA plot we found that the new PC1' corresponded primarily to differences in drug dose and PC2' to differences in time of exposure (Fig. 2C); this can be visualized by projecting PC1' and PC2' loadings onto the experimental design, as shown to the right of the PCA plots. When we generated rotated PCA plots for the four TKIs individually, we observe that the correlation between dose and time was highest for Sorafenib. Genes repressed by high drug doses and short times or by lower drug doses at longer times are found in the lower left quadrant of Fig. 2E (denoted by a green box) whereas genes induced at high drug doses and short times or lower drug doses and longer times were found in the upper right quadrant (red box). For Sorafenib, the magnitude of gene induction under the two sets of conditions was similar (Fig. 2F; data for Sunitinib are shown in Supplementary Fig. 2C).

To confirm transcript expression changes observed by RNA-Seq using an independent method, 90 differentially expressed genes from a range of GO categories were analyzed using quantitative real-time PCR (qRT-PCR) (Supplementary Table 3). Three conditions (3 μM drug for 24 hr and 72 hr and 10 μM drug for 24 hr)

were assayed in triplicate, yielding a total of 42 samples. We found that the Pearson correlation for differential gene expression as measured using the two assays was 0.93 to 0.98 depending on the drug (Supplementary Fig. 2D). Overall, these data show that patterns of TKI-induced gene expression are reproducible over separate lots of Cor.4U cells and two different measurement methods. Moreover, for Sorafenib, and to a lesser extent for Sunitinib, it was the cumulative effect of dose and time of exposure that determined the magnitude of response, rather than dose or time individually. This observation increases the likelihood that analysis of cultured cells over short time periods (days) will be relevant to understanding longer duration exposure in patients (weeks to months).

Biological processes altered by TKI exposure

To identify biological processes altered by TKI exposure we analyzed RNA-Seq data using g-means clustering followed by *goseq* analysis. G-means clustering (Hamerly and Elkan, 2004) is an abstraction of k-means clustering that detects the optimal number of clusters using a hierarchical approach. Data in the neighborhood of a cluster is tested for its fit to a Gaussian distribution; if the data have a more complex distribution, the cluster is successively split until a Gaussian is achieved. When all data were pooled, G-means clustering identified 16 major clusters, 13 of which could be associated with significantly enriched GO terms. Many of these GO terms were associated with metabolism (*Amino acid metabolic process* GO:0006520, *Lipid biosynthetic process* GO:0008610, *Mitochondrion* GO:0005739) and some with contraction of muscle (*Sarcomere* GO:0030017). Some GO terms were enriched for a specific drug (e.g. *Intracellular part* GO: 0044424, *Ribosome biogenesis* GO:0042254, *Mitochondrion* GO:0005739 only by Sorafenib) but others were enriched for all drugs (e.g. genes in *Extracellular Space* GO:0005615 were consistently down-regulated and those for *Lipid biosynthetic process* GO:000861) were upregulated). Within these categories were multiple genes that had previously been implicated in cardiac biology or dysfunction. For example, steroid biosynthesis is elevated in cases of cardiac hypertrophy and progression to heart failure (Ohtani et al., 2009).

Given that RNA-Seq data were acquired for multiple drugs, doses, and times of treatment, a fairly diverse and complex set of changes is to be expected. To begin to identify common biological processes altered by TKI treatment, we selected the top 1-2 GO terms in each cluster and plotted the log2-fold change for the top 20 genes

in each GO term against the cruciform time-dose experimental design (Fig. 3). In the case of Sorafenib, expression changes at high dose and long times were consistent (recapitulating the data in Fig. 2), with *Sarcomere* GO:0030017 strongly down-regulated and *Ribosome biogenesis* GO:0042254 and *Cellular Amino Acid Metabolic Process* GO:0006520 strongly upregulated. We found no evidence of enrichment for GO terms associated with DNA damage. Moreover, when our data were combined with previously published signatures for anthracycline exposure of cardiac cells, PCA showed that the effects of TKIs and anthracyclines were distinct. Thus, while TKIs differ in their specific effects on hiPSC-CMs, we conclude that differentially regulated GO terms related to metabolism, biosynthetic processes and contractility were most often associated with overall drug exposure. This signature appears to be quite distinct from that of well-studied cardiotoxic drugs such as anthracyclines (Burridge et al., 2016).

Changes in protein levels following exposure of hiPSC-CMs to TKIs

TKI-induced changes in the proteome were monitored by mass spectrometry following labelling with 10 different isobaric Tandem Mass Tags (or TMTs) (Dayon and Sanchez, 2012). Cells were exposed to 3μM TKI for 24 or 72 hr and data from three batches of cells run as three separate TMT-experiments (30 samples total); these were combined by normalizing each drug treatment to a contemporaneous vehicle-only control (see STAR METHOD). A total of 7,727 proteins were detected in the union of the three experiments. PCA analysis showed that PC1 differentiated early and late samples, whereas PC2 distinguished between Sorafenib, Sunitinib, and Lapatinib. Erlotinib induced relatively small deviations from the DMSO-only control and replicate samples for all drugs clustered close to each other, demonstrating good reproducibility (Fig. 4A; Supplementary Fig. 3). Differentially regulated proteins were identified using a one-way ANOVA test (with correction for multiple hypothesis testing set to FDR $\leq$ 0.05 and fold change $\geq$ 1.2). In the case of Sunitinib 562 differentially expressed proteins were detected at t = 72 hours in contrast to 90 proteins for Erlotinib-treated cells (Supplementary Fig. 4A). The data were clustered using K-means clustering with k = 11; adding more clusters did not significantly reduce the total within-cluster sum of squares (Supplementary Fig. 4B). Proteins in several clusters were drug-specific; for example, proteins in Cluster 1 (*Peroxisome* GO:0005777) were down-regulated by Lapatinib alone,

and proteins in Cluster 6 (*Extracellular matrix component* GO:0044420) were down-regulated following exposure to Sorafenib but up-regulated by the other three drugs. However, terms associated with amino acid metabolism, lipid metabolic process, sarcomere, mitochondrion, extracellular matrix, and ribosomal function were all differentially regulated in multiple drugs.

Integrating mRNA and proteomic data

TKIs typically inhibit multiple enzymes with similar affinity; Sorafenib and Sunitinib have particularly broad poly-pharmacology. Of the 537 human kinases as described in KinMap (Eid et al., 2017), 77% appear to be expressed in Cor.4U hiPSC-CMs: mRNA and protein were detected for 274 kinases, mRNA alone for 136 kinases and protein alone for 6 kinases (Supplementary Table 5). Kinases were among the differentially regulated genes or proteins observed for all four TKIs, including drug targets in some cases: ERBB2 protein, a primary target of Lapatinib, increased in response to Lapatinib treatment whereas the levels of VEGFR1 (FLT1) protein fell in response to Sorafenib treatment. By comparing our data to profiling studies that describe the full range of TKI on- and off-target binders (Davis et al., 2011) we estimate that ~143 potential targets for Sunitinib are expressed in Cor.4U cells as are 25 potential targets for Sorafenib, 5 for Lapatinib and 20 for Erlotinib (Supplementary Fig. 5).

Many more genes were detected by RNA-Seq than by proteomics (across all conditions, 12,001 coding genes vs. 7,727 proteins). To compare the two data sets we focused on the 6151 genes detected by both assays. PCA of differentially expressed genes (DEGs) detected by both RNA-Seq and proteomics revealed broadly consistent changes following TKI exposure, (Supplementary Fig. 6E) even though the number of overlapping differentially expressed genes was low. Following 3 μM Sunitinib treatment at 72 hr only 6% of DEGs (43 genes) were observed in both assays, and for Sorafenib only 7% of DEGs (98 genes) were observed in both (Supplementary Fig. 6B). However, among the few genes and proteins that did overlap, the Pearson correlation between changes in mRNA expression and changes in protein abundance was high ($r = 0.7$ to 1 depending on the drug). However, at the level of GO term enrichment, terms associated with mitochondrial biology, metabolism and sarcomere function were common to both RNA-Seq and proteomic data. Moreover, we found that DEGs from mRNA or proteomic data mapped to multiple successive steps in a biosynthetic pathway even when the

degree of correlation between protein and RNA was not high. This is illustrated in Supplementary Fig. 6C for enzymes in the cholesterol biosynthetic pathway that were upregulated following exposure of Cor.4U cells to Lapatinib and in Supplementary Fig. 6D for components of sarcomere that were down-regulated following exposure to Sorafenib. These patterns are potentially interesting for follow-up studies aimed at better understanding the regulation of the specialized metabolism of cardiac cells.

Functional analysis of TKI-induced changes in hiPSC-CM

To confirm the biological significance of TKI-induced changes in gene and protein expression in Cor.4U cells, we performed a functional analysis. First, we looked at proteins involved in peroxisome function and biogenesis, 18 of which were downregulated 2-fold or more by exposure to 3 µM Lapatinib for 72 hr. This change is detected in proteomic but not RNA-Seq data, implying post-transcriptional regulation of peroxisome protein abundance. When we performed immunofluorescence with antibodies against one of these proteins (PEX14) we found that the number of peroxisomes was reduced ~8-fold by Lapatanib treatment. Cardiac cells are particularly dependent on the oxidation of fatty acids for metabolic energy, and much of this oxidation takes place in peroxisomes (van der Vusse et al., 1992); thus, dramatic reductions in peroxisomes in hiPSC-CMs is likely to impose a substantial metabolic burden. Sunitinib and Sorafenib also reduced the expression of Troponin T2, an important component of sarcomeres, ~80-fold in proteomic data as compared to control cells (Fig. 5B) and consistent with an observed reduction in spontaneous beating. Thus, two striking molecular changes associated with TKI exposure have clear physiological consequences at the levels of organelle structure.

We focused our study of TKI-induced changes in metabolism on Sorafenib, which we observed downregulated multiple processes involved in mitochondrial electron transport (Fig. 3). Sorafenib has previously been shown to inhibit mitochondrial respiration in tumor cells, immortalized H9c2 rat myocardial cells, and mouse embryonic fibroblasts (Will et al., 2008; Zhang et al., 2017). To better understand the hiPSC-CM metabolic phenotype we measured mitochondrial oxygen consumption rate (OCR; using the Agilent Seahorse XF96 analyzer) in Cor.4U cells. Over the course of 12 minutes, we first measured basal respiratory capacity of cells, then treated them with oligomycin A, an ATP synthase inhibitor, to calculate ATP-coupled respiration. We

next added a mitochondrial uncoupler (FCCP) to measure maximal respiratory capacity. Finally, Rotenone and Antimycin A, (complexes I and complex III inhibitors, respectively), were added to fully block electron transport and reveal the rate of non-mitochondrial respiration, used to define the baseline for all calculations. Sustained treatment of Cor.4U cells with Sorafenib for 48 hr caused a dramatic impairment in mitochondrial function (Fig. 6B, compare red and green lines). Basal respiration was reduced 9-fold, ATP-coupled respiration was reduced 23-fold, and maximal respiratory capacity was 45-fold lower in Sorafenib treated than control cells. These changes are most likely a consequence of a coordinated reduction in the expression of multiple subunits of oxidative phosphorylation complexes, as had we observed in RNA-Seq data.

To determine whether mitochondrial defects caused by Sorafenib treatment were reversible, mitochondrial respiration was measured in cells that were exposed to 6 μM Sorafenib for 48 hr, followed by a recovery period of either 1 hr or 49 hr during which the drug was washed away and cells cultured in normal growth media (Fig. 6B, blue lines). The study was designed to control for total time in culture, for the duration of Sorafenib exposure, and for the switch (for 1 hr) from Cor.4U growth medium to the medium used to measure OCR (non-buffered DMEM; see Fig. 6A and Star Methods). A short recovery period (1 hr) was sufficient to restore basal respiration in the treated cells. However, unlike control cells, respiration was not coupled to ATP production (as evidenced by the lack of an effect upon oligomycin addition). After 49 hr of recovery in the absence of Sorafenib, mitochondrial functions were largely recovered. However, maximal respiratory capacity was lower in the cells previously exposed to the drug as compared to control cells. Thus, the effects of Sorafenib on mitochondrial function are largely reversible following withdrawal of drug. The different time scales of recovery for basal respiration and ATP production, and evidence of proton leakage following 1 hr of recovery, suggest that more than one inhibitory mechanism is involved. We speculate that proteins directly inhibited by Sorafenib binding (likely to include ATPases other than kinases) may recover activity on a rapid time-scale whereas proteins down-regulated at a transcriptional level may take longer to regain function.

Exposing hiPSC-CMs to Sorafenib results in an adaptive response involving increased glycolysis

Glycolysis is an alternative means of producing ATP when mitochondrial function is impaired. Sorafenib treatment was observed to cause an increase in the extracellular acidification rate (ECAR; also measured using a Seahorse XF96 analyzer), an indirect measure of glycolysis (Fig. 7A). We also detected a large decrease in glucose concentration and an increase in lactate concentration in the growth media of cells treated with Sorafenib, compared to control; these changes are also characteristic of a glycolytic shift (Fig. 7B). Thus, hiPSC-CMs compensate for inhibition of mitochondrial function by upregulating glycolysis, a shift that would normally be observed in the heart when cells are starved for oxygen (fetal heart cells also utilize glycolysis more heavily than adult cells). Evidence of significant glycolytic shift was also found in metabolic profiling of cells treated with Sorafenib, as measured using hydrophilic interaction liquid chromatography tandem mass spectrometry (HILIC-MS; Supplementary Fig. 7B; (Spinelli et al., 2017)).

To determine whether the glycolytic shift in hiPSC-CMs is important for cell viability, we treated cells with DMSO or Sorafenib at a range of doses (1-10 μM) for 48 hr to induce the glycolytic phenotype. Cells were then treated with 2-deoxy-D-glucose (2DG; a non-metabolizable glucose analog that competitively inhibits hexokinase) in combination with Sorafenib for another 48 hr. We then measured ATP levels by Cell-Titer Glo (Fig. 7B and C). As controls, we assayed the effect of 2DG treatment alone and of 2DG plus Sorafenib in the absence of Sorafenib pre-treatment. The culture media for hiPSC-CMs contains ~25mM glucose and we therefore tested 2DG over a 0-32 mM concentration range. As expected, 2DG alone inhibited metabolism in a dose-dependent manner, reducing ATP levels to ~60% of their control levels after 48 hr in the presence of 32 mM 2DG (Supplementary Fig. 7A; unexpectedly, co-treatment of cells with 2DG reduced the impact of 10 μM Sorafenib on ATP levels; the reasons for this are unknown but we note that hiPSC-CMs rapidly lose viability in 10 μM Sorafenib). To determine whether the shift to glycolysis at lower Sorafenib doses was physiologically important, we divided the observed effect of Sorafenib plus 2DG by the effect of 2DG alone in the presence and absence of pre-treatment. Following simultaneous exposure to 2DG and Sorafenib across a range of doses, little change in ATP level was observed compared to 2DG alone. However, when cells were pre-treated with 3 or 6 μM Sorafenib the effect on ATP levels was significantly greater (highlighted in yellow in Fig. 7C). These data suggest that the

observed glycolytic shift is an adaptive response that is necessary for cardiomyocytes to maintain their metabolic activity in the presence of Sorafenib.

DISCUSSION

In this paper we profile changes in gene and protein expression and the physiology of hiPSC-CMs following exposure to four tyrosine kinase inhibitors used to treat diverse solid tumors. The long-term goal is to understand and eventually mitigate TKI-mediated cardiotoxicity using changes in dosing strategies and co-drugging with cardioprotective agents. Cultured cells do not recapitulate many of the features of cardiac tissue, but they are nonetheless well-established as a means to study molecular mechanisms relevant to cardiac biology and disease (e.g. neonatal rat ventricular myocytes in the study of cardiac hypertrophy) (Harvey and Leinwand, 2011). Cardiomyocytes differentiated from iPSCs are a more physiologically relevant cell type than rodent cells and are more manipulable than whole animals: hiPSC-CMs are post-mitotic, have well-developed sarcomeres and beat spontaneously *in vitro*. However, they have some limitations, including molecular properties midway between fetal and adult cells and – in this study – growth in biologically unrealistic culture conditions (conditions which greatly facilitate molecular profiling). We find that many of the kinases targeted by TKIs are expressed in cardiac cells. These kinases, and the signaling pathways in which they operate, are known from other studies to be important for cardiomyocyte physiology (Chen et al., 2008b). Inhibition of signaling kinases results in cell cycle arrest and killing of cancer cells and similar activities are postulated to be the cause of TKI-induced cardiotoxicity (Cheng and Force, 2010; Force et al., 2007). However, we find that TKIs induce wide-spread reprogramming of gene expression in hiPSC-CMs under conditions in which little or no cell death is observed. Proliferative arrest, an activity of most anti-cancer drugs, is also not physiologically relevant to mature cardiomyocytes and is observed in Cor.4U cultures only in the subset of cells (5-10%) that are not differentiated. We observe many changes in gene expression previously observed in studies more focused on TKI-treated cardiomyocytes, including Sorafenib-mediated up-regulation of ER stress genes (e.g. DDIT3, ATF3 and CHAC1; (Dixon et al., 2014) and changes in the expression of VEGF proteins (e.g. KDR and VEGFC; (Sharma et al., 2017). Lapatinib causes widespread upregulation of cholesterol biosynthetic enzymes ((Necela et al., 2017); Supplementary Fig.

6C). Cell cycle genes are also down-regulated when hiPSC-CMs cultures are exposed to TKIs, but this this is likely caused by arrest of a subset of undifferentiated Cor.4U cells as described above. Across our dataset, the most widely misregulated GO processes are those associated with metabolism, biosynthesis, and remodeling of the extracellular environment. In addition to inducing cholesterol biosynthetic enzymes, Laptinib exposure downregulates multiple peroxisomal proteins and dramatically reduces peroxisome number. Since peroxisomes play an important role in cholesterol biosynthesis and homeostasis, the two biological pathways affected by Lapatinib may be connected: upregulation of cholesterol pathway enzymes may be a response to loss of peroxisomal biosynthetic capacity.

The most profound metabolic defect that we have studied functionally is Sorafenib-dependent inhibition of mitochondrial ATP production. The adult myocardium is highly active metabolically and 95% of its energy derives from oxidative phosphorylation in mitochondria fueled by fatty acyl-coenzyme A. The effect of Sorafenib on mitochondria is reversible upon drug withdrawal (as is Sorafenib cardiotoxicity in human patients (Uraizee et al., 2011)) and probably exploits the normal ability of cardiomyocytes to switch energy source as a function of developmental stage and oxygen tension (Breckenridge et al., 2013; Gong et al., 2015). Induction of glycolysis reduces the toxicity of Sorafenib, presumably by providing an alternative source of ATP. By analogy, sensitivity to Sorafenib in hepatocellular carcinoma cells (Tesori et al., 2015) is negatively correlated with reliance on glycolysis (Shen et al., 2013). However, increased reliance on glycolysis is also a characteristic of cardiac hypertrophy, myocardial ischemia and cardiac failure (Rosano et al., 2008; Ventura-Clapier et al., 2004)(Doenst et al., 2013). Sorafenib and other TKIs have been observed to reduce blood glucose levels (Agostino et al., 2011), potentially enhancing the adverse consequences of a reliance on glycolysis for energy. In the short-term, the switch in Sorafenib-treated hiPSC-CMs from oxidative phosphorylation to glycolysis represents a form of adaptive drug resistance, but longer term effects in patients may represent a physiological liability. We propose that the cardiotoxicity of Sorafenib might be caused in large part by metabolic remodeling rather than by inhibition of immediate-early signaling, as previously suggested (Force et al., 2007).

Drug dose and time of exposure are key pharmacological variables but they are often ignored in genome-wide profiling studies because each condition is expensive to analyze. We used simple functional assays

(mitochondrial membrane potential and ATP production) across a wide-range of exposure times and concentrations spanning the C_{max} value to identify conditions that elicited a scorable cellular phenotype but not cell killing. For Lapatinib, Erlotinib, and Sorafenib the optimal *in vitro* concentration was similar to or below the C_{max} value in humans, but for Sunitinib it was 10-fold higher; why this is true is not clear, but effective drug concentrations for tumor cells also differ in many cases from those *in vivo*. Through profiling experiments we explored both dose and time using a relatively compact design of six conditions. The use of multiple lots of cells was nonetheless required and experimentation spanned a period of ~18 months. However, we found that the molecular profiles of Cor.4U cells from different lot numbers were highly correlated, making it possible to assemble a dataset without strong batch effects. Moreover, because Cor.4U cells are commercially available, it should be possible for others to design experiments based on our data (all of which is annotated to NIH LINCS standards and deposited on Synapse (Synapse ID: syn7079983)). Examining the data as a whole we find that, for some drugs and molecular processes (as defined by enriched GO terms), total exposure is the key variable: enriched genes under high-dose and short time conditions are highly correlated with those at lower dose and longer time (this includes the metabolism-linked changes described above). In these cases, it seems more likely that *in vitro* studies spanning a period of days will be relevant to understanding human exposure spanning a period of weeks to months.

The data in this paper represent a resource for generating network-level hypotheses about drug-induced cardiotoxicity. We have mined only a small subset of the gene enrichment and GO data, and validated only peroxisomal, sarcomere and mitochondrial phenotypes. Deeper analysis of these phenomena is clearly warranted in Cor.4U cells and potentially also in cells derived from patients with cardiac dysfunction. The adaptive drug resistance we observed for mitochondrial metabolism during Sorafenib treatment is particularly intriguing. Adaptive resistance has been most extensively studied in tumor cells and combination therapies are being developed to block adaptation and increase tumor cell killing. In the case of cardiomyocytes, blocking adaptation or decreasing blood glucose levels by indirect means is expected to increase the adverse effects of Sorafenib. Thus, managing drug-induced cardiotoxicity will need to focus not just on acute on-target effects of drug exposure, but also adaptive and maladaptive physiological responses.

Acknowledgments

We thank J. Lin, R. Jiang, A. Jenney at the LSP, A. Moreno in the Haigis lab and Qiagen Lifesciences Service Core for analysis and experimental assistance. This manuscript is dedicated to Darrell Abernathy MD, PhD, Associate Director for Drug Safety in the Office of Clinical Pharmacology at the FDA, who inspired and guided this work until his untimely death. The research was supported by a FDA contract HHSF223201400052C, NIH grant P50-GM107618 and a NIH LINCS grant U54-HL127365 to PKS, and by an American Heart Association postdoctoral fellowship 15POST25230014 and a NIH F32 HL14223 to HW.

Author Contributions

HW, LM and PKS conceived study. HW performed the experiments and analysis except as follows: SAB performed RNA-Seq library preparation. RAE performed the mass spectrometry experiment and data preprocessing. NRH profiled media metabolite under the supervision of MCH. CAJ performed immunofluorescence. RPS performed gmeans analysis and ACP performed principal component analysis for the RNA-Seq data, KMH provided the original code in edgeR and goseq analysis. HW, RPS and PKS wrote the paper.

Competing Financial Interests:

The authors declare no competing financial interests.

FIGURE LEGENDS

Figure 1: Phenotypic responses of human iPSC-derived cardiomyocytes to four TKIs. (**A**) Cor.4U cells were cultured in vendor-specified growth media containing 10% FBS for 3 days, switched into a second vendor-specified media plus 1% FBS for 1.5 days and then exposed to drugs; for phenotypic studies, TKI doses between 0.1 -10 µM and treatment times between 6 hours and 7 days (25 in total) were examined. (**B**) Cor4U cells were stained with □-actinin (green), Troponin T2 (red) and DAPI for nuclei (blue) and imaged by DeltaVision Elite. Images show a representative cell from three independent experiments (see Fig. S1 for lower magnification). (**C**) Mitochondrial membrane potentials of iPSC-CMs across 25 conditions for four TKIs. Values were normalized to those of cells treated with DMSO alone for the same amount of time. (**D**) ATP levels of whole-cell extracts measured using the Cell Titer Glo assay; conditions were the same as in Panel C.

Figure 2: Responses of hiPSC-CMs to four TKIs as measured by RNA-Seq. (**A**) Three independent experiments with different lots of Cor.4U cells were required for the study. Drug treatment followed a cruciform design involving 1, 3 or 10 µM drug for 24 hr and 3 µM drug for additional three time points (6, 72 and 168 hr). A total of 84 RNA samples were sequenced on a HiSeq 2500 yielding ~13,000 mapped transcripts per sample. (**B**) Principal component analysis (PCA) on fold-change values from RNA-Seq. (**C**) The same data as in B with the axes rotated by □=45° with was observed to optimally place dose along PC1' and time along PC2' (see loadings to right); inset shows the directions of the original PCs. (**D**) Scores of drug-induced gene expression changes were plotted against PC1' and PC2'. (**E**) For the Sorafenib data in Panel D, genes corresponding to different dose-time regimes were selected (colored boxes I to IV) and the average gene expression changes were plotted on the experimental design (**F**) Representative changes in expression for genes falling in boxes II-A and II-B from Panel E; each line represents one gene and colors are arbitrary.

Figure 3: Effect of TKIs on the transcriptome across dose and time. Gene expression data were clustered by G-means clustering, which yielded 16 clusters, 13 of which had enriched GO terms. The top GO term(s) is shown

for each cluster, with 20 representative genes from that cluster plotted in each box of the cruciform experimental design in Figure 2A. Color scale is based on log2-transformed fold-changes.

Figure 4: Effect of TKIs on the proteome across dose and time. (A) PCA of changes in protein levels for four TKIs at two timepoints; two biological replicates were collected for each condition (20 samples in total including DMSO-only control). Data were pooled after calculating log2-transformed fold-changes in protein levels relative to DMSO at the corresponding time point. Arrows depict the direction of change associated with each drug. (**B**) Proteomic fold-change data was clustered by k-means clustering with k = 11; the top GO terms for each cluster are shown in Supplementary Table 6. Magnified views to right show individual genes for three enriched GO terms in these clusters. (**C**) GO terms enriched for genes that were significantly regulated at both RNA and protein levels by any drug; redundancy in the list of GO terms was eliminated to simplify the representation.

Figure 5: Protein expression changes confirmed by immunofluorescence.

(**A**) Staining of Peroxisomal Biogenesis Factor 14 (PEX14) in hiPSC-CMs treated with DMSO alone or with 3 µM Lapatinib for 3 days. Low and high magnifications are shown. (**B**) Staining for cardiac isoforms of Troponin T (TNNT2) in hiPSC-CMs treated with a DMSO alone or with 3 µM Sunitinib or Sorafenib at for 4 days. Experiments in Panels A and B were repeated three times and images shown are representative of a single experiment.

Figure 6: Effect of Sorafenib on mitochondrial respiration in hiPSC-CMs. (A) Design of experiments testing the effect of Sorafenib mitochondrial respiration. The two controls differ in whether or not Sorafenib was preset in the assay medium. **(B)** Oxygen consumption rate (OCR) in live hiPSC-CMs was measured at baseline and following successive addition of Oligomycin A, FCCP and Rotenone plus Antimycin A (see text for details). Conditions correspond to those described in Panel A. This experiment was repeated twice with 6 replicates per condition in each experiment; data were the average from these two experiments. Error bars are standard error with n = 2. **(C)** Metabolic parameters derived from analysis of the OCR data shown in Panel B**.** Error bars are

standard error with n = 2. **(D)** Genes involved in Oxidative Phosphorylation that were down-regulated as measured by RNA-Seq in cells exposed to 10 µM Sorafenib for 24 hr.

Figure 7: Induction of glycolysis by Sorafenib in hiPSC-CMs. (**A**) Panel on left: Extracellular acidification rate (EAR) measured for hiPSC-CMs cells treated with a DMSO alone or 3 µM Sorafenib for 2 days. Error bars show the standard deviation of one experiment having 6 biological replicates per condition. Data is a representative of study performed three times. The unit of y-axis is mpH/min/1000 cells. Panels on right: The levels of glucose and lactate measured in spent media collected from cells treated with a DMSO alone or 3 µM Sorafenib for 1-5 days. Error bars show the standard error of three independent experiments. (**B**) Design of a co-drugging experiment examining the impact of Sorafenib-induced glycolysis on sensitivity to Sorafenib, as measured using the Cell Titer Glo luminescence assay. In the "pre-treatment phase," cells were exposed to 0-10 µM Sorafenib for 48 hr and then shifted to an "assay phase" in which cells were incubated in a combination of 0-32 µM 2-deoxy-D-glucose (2DG) and 0-10 µM Sorafenib for 48 hr prior to measurement of ATP levels. (**C**) Normalized ATP levels of cells subjected to the experiment described in Panel B. Data were normalized to luminescence values of cells treated with 2DG alone at the specified doses (see Supplementary Fig. 7A). Each dot represents the average of 3-8 replicates in each of the two independent experiments and error bars are the standard error of two independent experiments (n=2).

LITERATURE CITED

Agostino, N.M., Chinchilli, V.M., Lynch, C.J., Koszyk-Szewczyk, A., Gingrich, R., Sivik, J., and Drabick, J.J. (2011). Effect of the tyrosine kinase inhibitors (sunitinib, sorafenib, dasatinib, and imatinib) on blood glucose levels in diabetic and nondiabetic patients in general clinical practice. J. Oncol. Pharm. Pract. *17*, 197–202.

Bhargava, P. (2009). VEGF kinase inhibitors: how do they cause hypertension? Am J Physiol Regul Integr Comp Physiol *297*, R1.

Blinova, K., Stohlman, J., Vicente, J., Chan, D., Johannesen, L., Hortigon-Vinagre, M.P., Zamora, V., Smith, G., Crumb, W.J., Pang, L., et al. (2017). Comprehensive Translational Assessment of Human-Induced Pluripotent Stem Cell Derived Cardiomyocytes for Evaluating Drug-Induced Arrhythmias. Toxicol. Sci. Off. J. Soc. Toxicol. *155*, 234–247.

Breckenridge, R.A., Piotrowska, I., Ng, K.-E., Ragan, T.J., West, J.A., Kotecha, S., Towers, N., Bennett, M., Kienesberger, P.C., Smolenski, R.T., et al. (2013). Hypoxic Regulation of Hand1 Controls the Fetal-Neonatal Switch in Cardiac Metabolism. PLOS Biol. *11*, e1001666.

Bresalier, R.S., Sandler, R.S., Quan, H., Bolognese, J.A., Oxenius, B., Horgan, K., Lines, C., Riddell, R., Morton, D., Lanas, A., et al. (2005). Cardiovascular events associated with rofecoxib in a colorectal adenoma chemoprevention trial. N. Engl. J. Med. *352*, 1092–1102.

Burridge, P.W., Li, Y.F., Matsa, E., Wu, H., Ong, S., Sharma, A., Holmström, A., Chang, A.C., Coronado, M.J., Ebert, A.D., et al. (2016). Human Induced Pluripotent Stem Cell–Derived Cardiomyocytes Recapitulate the Predilection of Breast Cancer Patients to Doxorubicin–Induced Cardiotoxicity. Nat. Med. *22*, 547–556.

Chen, M.H., Kerkelä, R., and Force, T. (2008). Mechanisms of Cardiac Dysfunction Associated With Tyrosine Kinase Inhibitor Cancer Therapeutics. Circulation *118*, 84–95.

Cheng, H., and Force, T. (2010). Molecular Mechanisms of Cardiovascular Toxicity of Targeted Cancer Therapeutics. Circ Res *106*, 21.

Chu, T.F., Rupnick, M.A., Kerkela, R., Dallabrida, S.M., Zurakowski, D., Nguyen, L., Woulfe, K., Pravda, E., Cassiola, F., Desai, J., et al. (2007). Cardiotoxicity associated with tyrosine kinase inhibitor sunitinib. Www.Thelancet.Com *370*.

Davis, M.I., Hunt, J.P., Herrgard, S., Ciceri, P., Wodicka, L.M., Pallares, G., Hocker, M., Treiber, D.K., and Zarrinkar, P.P. (2011). Comprehensive analysis of kinase inhibitor selectivity. Nat Biotechnol *29*, 1046–1051.

Dayon, L., and Sanchez, J.C. (2012). Relative protein quantification by MS/MS using the tandem mass tag technology. Methods Mol Biol *893*, 115–127.

Doenst, T., Nguyen, T.D., and Abel, E.D. (2013). Cardiac metabolism in heart failure: implications beyond ATP production. Circ. Res. *113*, 709–724.

Dogan, E., Yorgun, H., Petekkaya, I., Ozer, N., Altundag, K., and Ozisik, Y. (2012). Evaluation of cardiac safety of lapatinib therapy for ErbB2-positive metastatic breast cancer: A single center experience. Med. Oncol. *29*, 3232–3239.

Eid, S., Turk, S., Volkamer, A., Rippmann, F., and Fulle, S. (2017). KinMap: a web-based tool for interactive navigation through human kinome data. BMC Bioinformatics *18*, 16.

Escudier, B., Eisen, T., Stadler, W.M., Szczylik, C., Oudard, S., Siebels, M., Negrier, S., Chevreau, C., Solska, E., Desai, A.A., et al. (2007). Sorafenib in Advanced Clear-Cell Renal-Cell Carcinoma. N. Engl. J. Med. *356*, 125–134.

Force, T., Krause, D.S., and Van Etten, R.A. (2007). Molecular mechanisms of cardiotoxicity of tyrosine kinase inhibition. Nat Rev Cancer *7*, 332–344.

Francis, J., Ahluwalia, M.S., Wetzler, M., Wang, E., Paplham, P., Smiley, S., McCarthy, P.L., Cohen, I.L., Spangenthal, E., and Battiwalla, M. (2010). Reversible cardiotoxicity with tyrosine kinase inhibitors. Clin. Adv. Hematol. Oncol. HO *8*, 128–132.

Gavila, J., Seguí, M.Á., Calvo, L., López, T., Alonso, J.J., Farto, M., and Sánchez-de la Rosa, R. (2017). Evaluation and management of chemotherapy-induced cardiotoxicity in breast cancer: a Delphi study. Clin. Transl. Oncol. *19*, 91–104.

Geyer, C.E., Forster, J., Lindquist, D., Chan, S., Romieu, C.G., Pienkowski, T., Jagiello-Gruszfeld, A., Crown, J., Chan, A., Kaufman, B., et al. (2006). Lapatinib plus Capecitabine for HER2-Positive Advanced Breast Cancer. N. Engl. J. Med. *355*, 2733–2743.

Gong, G., Song, M., Csordas, G., Kelly, D.P., Matkovich, S.J., and Dorn, G.W. (2015). Parkin-mediated mitophagy directs perinatal cardiac metabolic maturation in mice. Science *350*, aad2459.

Hamerly, G., and Elkan, C. (2004). Learning the k in k-means. In Advances in Neural Information Processing Systems 16, S. Thrun, L.K. Saul, and P.B. Schölkopf, eds. (MIT Press), pp. 281–288.

Harvey, P.A., and Leinwand, L.A. (2011). Cellular mechanisms of cardiomyopathy. J. Cell Biol. *194*, 355–365.

Johnson, D.B., Balko, J.M., Compton, M.L., Chalkias, S., Gorham, J., Xu, Y., Hicks, M., Puzanov, I., Alexander, M.R., Bloomer, T.L., et al. (2016). Fulminant Myocarditis with Combination Immune Checkpoint Blockade. N Engl J Med *375*, 1749–1755.

Karakikes, I., Ameen, M., Termglinchan, V., and Wu, J.C. (2015). Human Induced Pluripotent Stem Cell-Derived Cardiomyocytes: Insights into Molecular, Cellular, and Functional Phenotypes. Circ. Res. *117*, 80–88.

Kerkela, R., Grazette, L., Yacobi, R., Iliescu, C., Patten, R., Beahm, C., Walters, B., Shevtsov, S., Pesant, S., Clubb, F.J., et al. (2006). Cardiotoxicity of the cancer therapeutic agent imatinib mesylate. Nat Med *12*, 908–916.

Kerkela, R., Woulfe, K.C., Durand, J.-B., Vagnozzi, R., Kramer, D., Chu, T.F., Beahm, C., Chen, M.H., and Force, T. (2009). Sunitinib-Induced Cardiotoxicity Is Mediated by Off-Target Inhibition of AMP-Activated Protein Kinase. Clin Transl Sci *2*, 15–25.

Magdy, T., Schuldt, A.J.T., Wu, J.C., Bernstein, D., and Burridge, P.W. (2018). Human Induced Pluripotent Stem Cell (hiPSC)-Derived Cells to Assess Drug Cardiotoxicity: Opportunities and Problems. Annu. Rev. Pharmacol. Toxicol. *58*, null.

Moslehi, J.J., and Deininger, M. (2015). Tyrosine Kinase Inhibitor–Associated Cardiovascular Toxicity in Chronic Myeloid Leukemia. J Clin Oncol *33*, 4210–4218.

Moslehi, J.J., Salem, J.-E., Sosman, J.A., Lebrun-Vignes, B., and Johnson, D.B. (2018). Increased reporting of fatal immune checkpoint inhibitor-associated myocarditis. The Lancet *391*, 933.

Motzer, R.J., Hutson, T.E., Tomczak, P., Michaelson, M.D., Bukowski, R.M., Rixe, O., Oudard, S., Negrier, S., Szczylik, C., Kim, S.T., et al. (2007). Sunitinib versus interferon alfa in metastatic renal-cell carcinoma. N Engl J Med *356*, 115–124.

Narayan, V., Keefe, S., Haas, N., Wang, L., Puzanov, I., Putt, M., Catino, A., Fang, J., Agarwal, N., Hyman, D., et al. (2017). Prospective Evaluation of Sunitinib-Induced Cardiotoxicity in Patients with Metastatic Renal Cell Carcinoma. Clin. Cancer Res. Off. J. Am. Assoc. Cancer Res. *23*, 3601–3609.

Necela, B.M., Axenfeld, B.C., Serie, D.J., Kachergus, J.M., Perez, E.A., Thompson, E.A., and Norton, N. (2017). The antineoplastic drug, trastuzumab, dysregulates metabolism in iPSC-derived cardiomyocytes. Clin. Transl. Med. *6*, 5.

Ohtani, T., Mano, T., Hikoso, S., Sakata, Y., Nishio, M., Takeda, Y., Otsu, K., Miwa, T., Masuyama, T., Hori, M., et al. (2009). Cardiac steroidogenesis and glucocorticoid in the development of cardiac hypertrophy during the progression to heart failure. J. Hypertens. *27*, 1074–1083.

Orphanos, G.S., Ioannidis, G.N., and Ardavanis, A.G. (2009). Cardiotoxicity induced by tyrosine kinase inhibitors. Acta Oncol. *48*, 964–970.

Perez, E.A., Koehler, M., Byrne, J., Preston, A.J., Rappold, E., and Ewer, M.S. (2008). Cardiac safety of lapatinib: pooled analysis of 3689 patients enrolled in clinical trials. Mayo Clin Proc *83*, 679–686.

Robinson, E.S., Khankin, E.V., Karumanchi, S.A., and Humphreys, B.D. (2010). Hypertension induced by vascular endothelial growth factor signaling pathway inhibition: mechanisms and potential use as a biomarker. Semin. Nephrol. *30*, 591–601.

Roden, D.M. (2004). Drug-induced prolongation of the QT interval. N. Engl. J. Med. *350*, 1013–1022.

Rosano, G.M., Fini, M., Caminiti, G., and Barbaro, G. (2008). Cardiac metabolism in myocardial ischemia. Curr Pharm Des *14*, 2551–2562.

Schmidinger, M., Zielinski, C.C., Vogl, U.M., Bojic, A., Bojic, M., Schukro, C., Ruhsam, M., Hejna, M., and Schmidinger, H. (2008). Cardiac Toxicity of Sunitinib and Sorafenib in Patients With Metastatic Renal Cell Carcinoma. J Clin Orthod *26*, 5204–5212.

Sharma, A., Burridge, P.W., McKeithan, W.L., Serrano, R., Shukla, P., Sayed, N., Churko, J.M., Kitani, T., Wu, H., Holmström, A., et al. (2017). High-throughput screening of tyrosine kinase inhibitor cardiotoxicity with human induced pluripotent stem cells. Sci. Transl. Med. *9*.

Shen, Y.C., Ou, D.L., Hsu, C., Lin, K.L., Chang, C.Y., Lin, C.Y., Liu, S.H., and Cheng, A.L. (2013). Activating oxidative phosphorylation by a pyruvate dehydrogenase kinase inhibitor overcomes sorafenib resistance of hepatocellular carcinoma. Br J Cancer *108*, 72–81.

Spinelli, J.B., Yoon, H., Ringel, A.E., Jeanfavre, S., Clish, C.B., and Haigis, M.C. (2017). Metabolic recycling of ammonia via glutamate dehydrogenase supports breast cancer biomass. Science *358*, 941–946.

Sun, C., Wang, L., Huang, S., Heynen, G.J.J.E., Prahallad, A., Robert, C., Haanen, J., Blank, C., Wesseling, J., Willems, S.M., et al. (2014). Reversible and adaptive resistance to BRAF(V600E) inhibition in melanoma. Nature *508*, 118–122.

Tesori, V., Piscaglia, A.C., Samengo, D., Barba, M., Bernardini, C., Scatena, R., Pontoglio, A., Castellini, L., Spelbrink, J.N., Maulucci, G., et al. (2015). The multikinase inhibitor Sorafenib enhances glycolysis and synergizes with glycolysis blockade for cancer cell killing. Sci. Rep. *5*, srep09149.

Uraizee, I., Cheng, S., and Moslehi, J. (2011). Reversible Cardiomyopathy Associated with Sunitinib and Sorafenib. N Engl J Med *365*, 1649–1650.

Vandenberg, J.I., Perry, M.D., Perrin, M.J., Mann, S.A., Ke, Y., and Hill, A.P. (2012). hERG K(+) channels: structure, function, and clinical significance. Physiol. Rev. *92*, 1393–1478.

Ventura-Clapier, R., Garnier, A., and Veksler, V. (2004). Energy metabolism in heart failure. J. Physiol. *555*, 1–13.

Von Hoff, D.D., Layard, M.W., Basa, P., Davis, H.L., Jr., Von Hoff, A.L., Rozencweig, M., and Muggia, F.M. (1979). Risk factors for doxorubicin-induced congestive heart failure. Ann Intern Med *91*, 710–717.

van der Vusse, G.J., Glatz, J.F., Stam, H.C., and Reneman, R.S. (1992). Fatty acid homeostasis in the normoxic and ischemic heart. Physiol. Rev. *72*, 881–940.

Waxman, A.J., Clasen, S., Hwang, W.-T., Garfall, A., Vogl, D.T., Carver, J., O'Quinn, R., Cohen, A.D., Stadtmauer, E.A., Ky, B., et al. (2018). Carfilzomib-Associated Cardiovascular Adverse Events: A Systematic Review and Meta-analysis. JAMA Oncol. *4*, e174519–e174519.

Will, Y., Dykens, J.A., Nadanaciva, S., Hirakawa, B., Jamieson, J., Marroquin, L.D., Hynes, J., Patyna, S., and Jessen, B.A. (2008). Effect of the multitargeted tyrosine kinase inhibitors imatinib, dasatinib, sunitinib, and sorafenib on mitochondrial function in isolated rat heart mitochondria and H9c2 cells. Toxicol. Sci. Off. J. Soc. Toxicol. *106*, 153–161.

Zhang, C., Liu, Z., Bunker, E., Ramirez, A., Lee, S., Peng, Y., Tan, A.C., Eckhardt, S.G., Chapnick, D.A., and Liu, X. (2017). Sorafenib Targets the Mitochondrial Electron Transport Chain Complexes and ATP Synthase to Activate the PINK1-Parkin Pathway and Modulate Cellular Drug Response. J. Biol. Chem. jbc.M117.783175.

Zhang, S., Liu, X., Bawa-Khalfe, T., Lu, L.-S., Lyu, Y.L., Liu, L.F., and Yeh, E.T.H. (2012). Identification of the molecular basis of doxorubicin-induced cardiotoxicity. Nat. Med. *18*, 1639–1642.

Figure 1

Figure 1

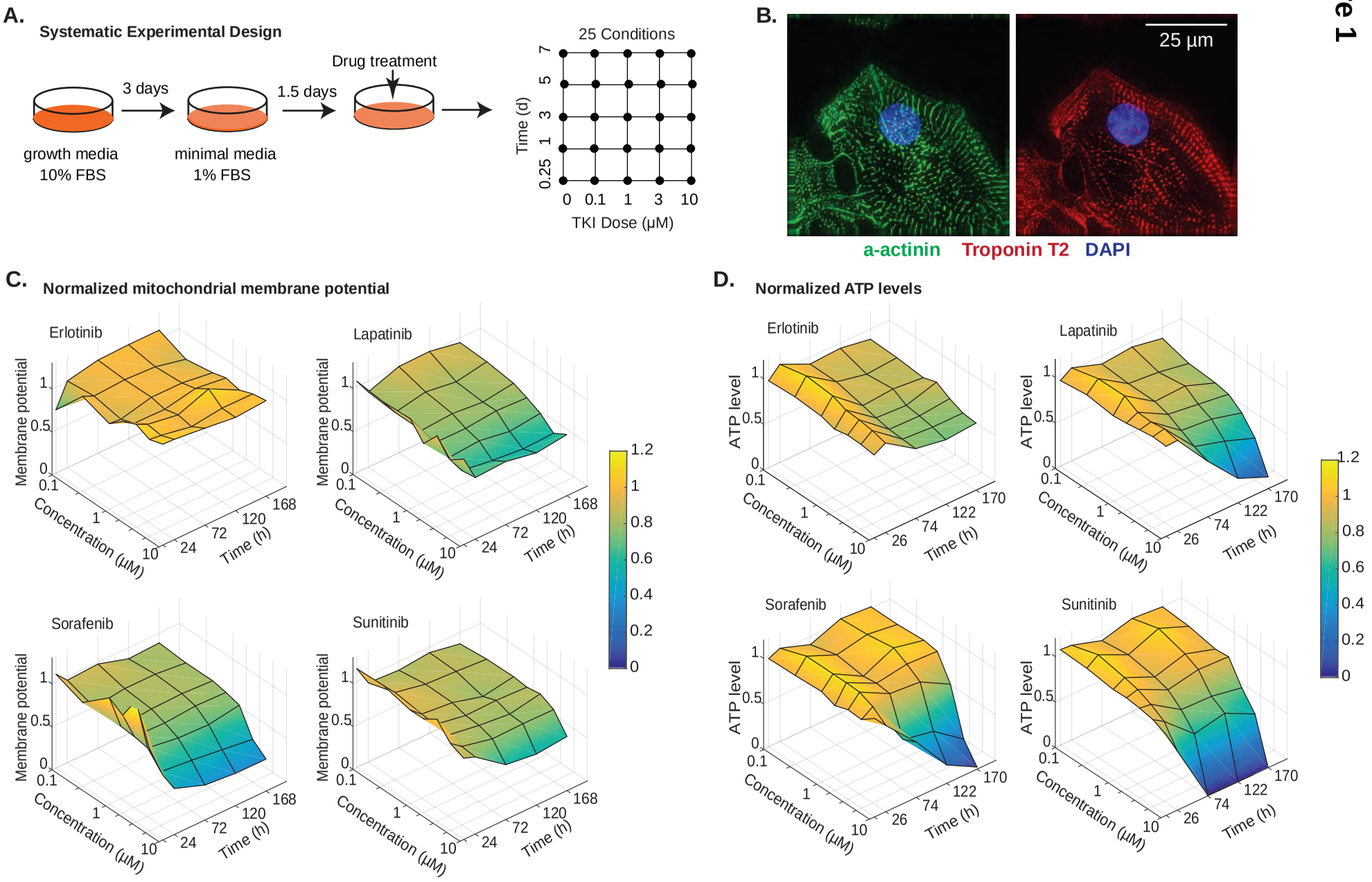

Figure 2

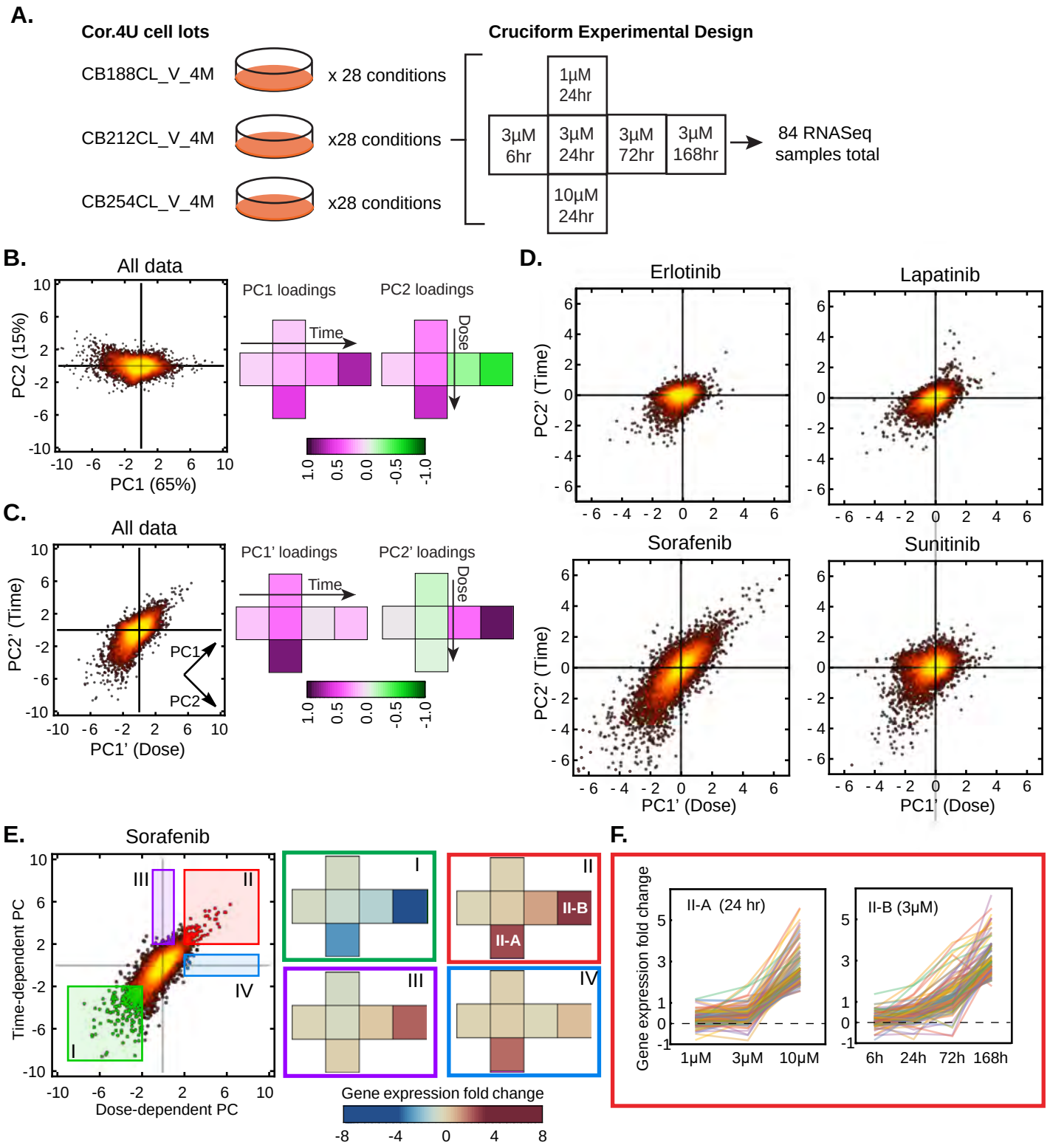

Figure 3

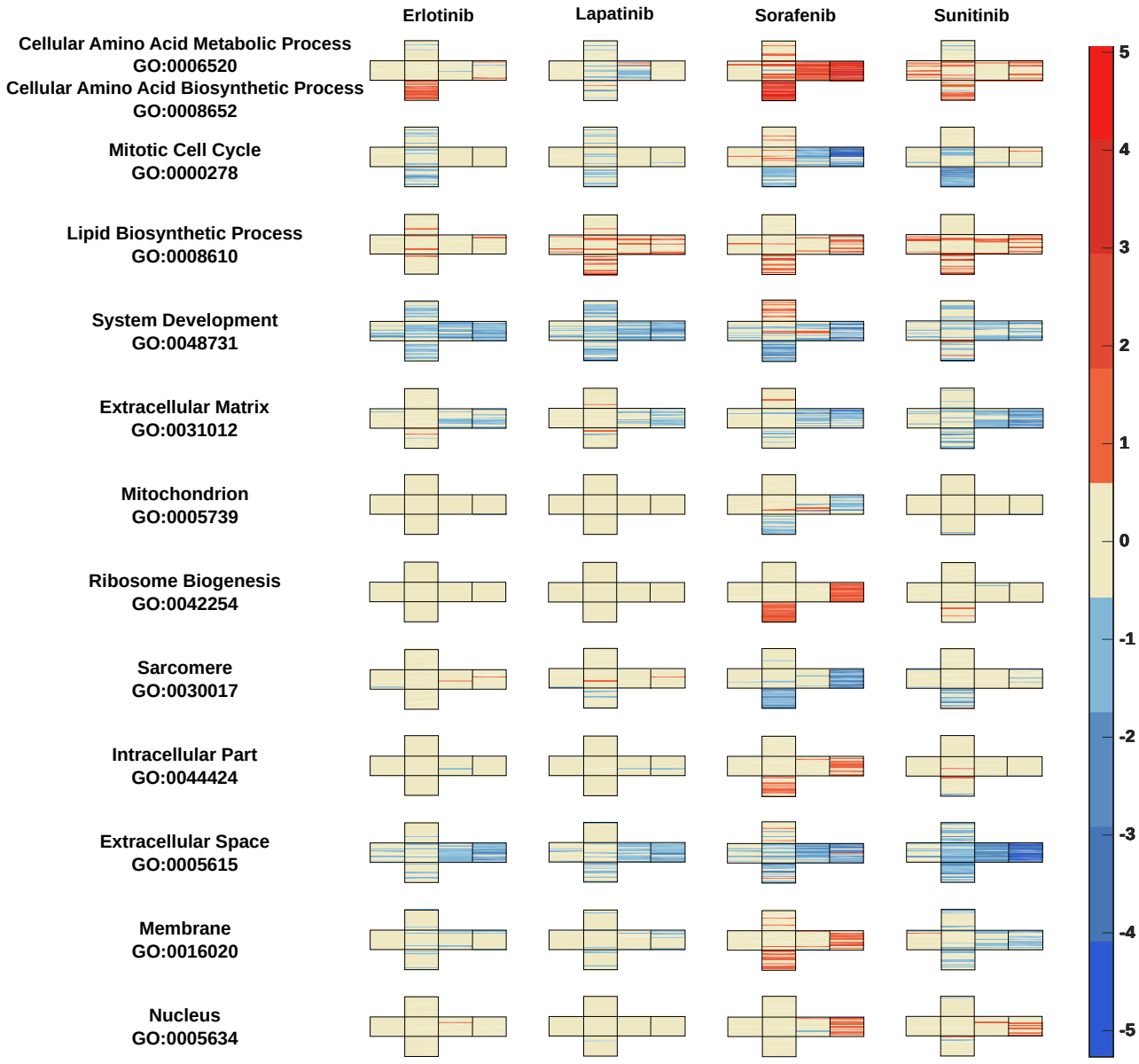

Figure 4

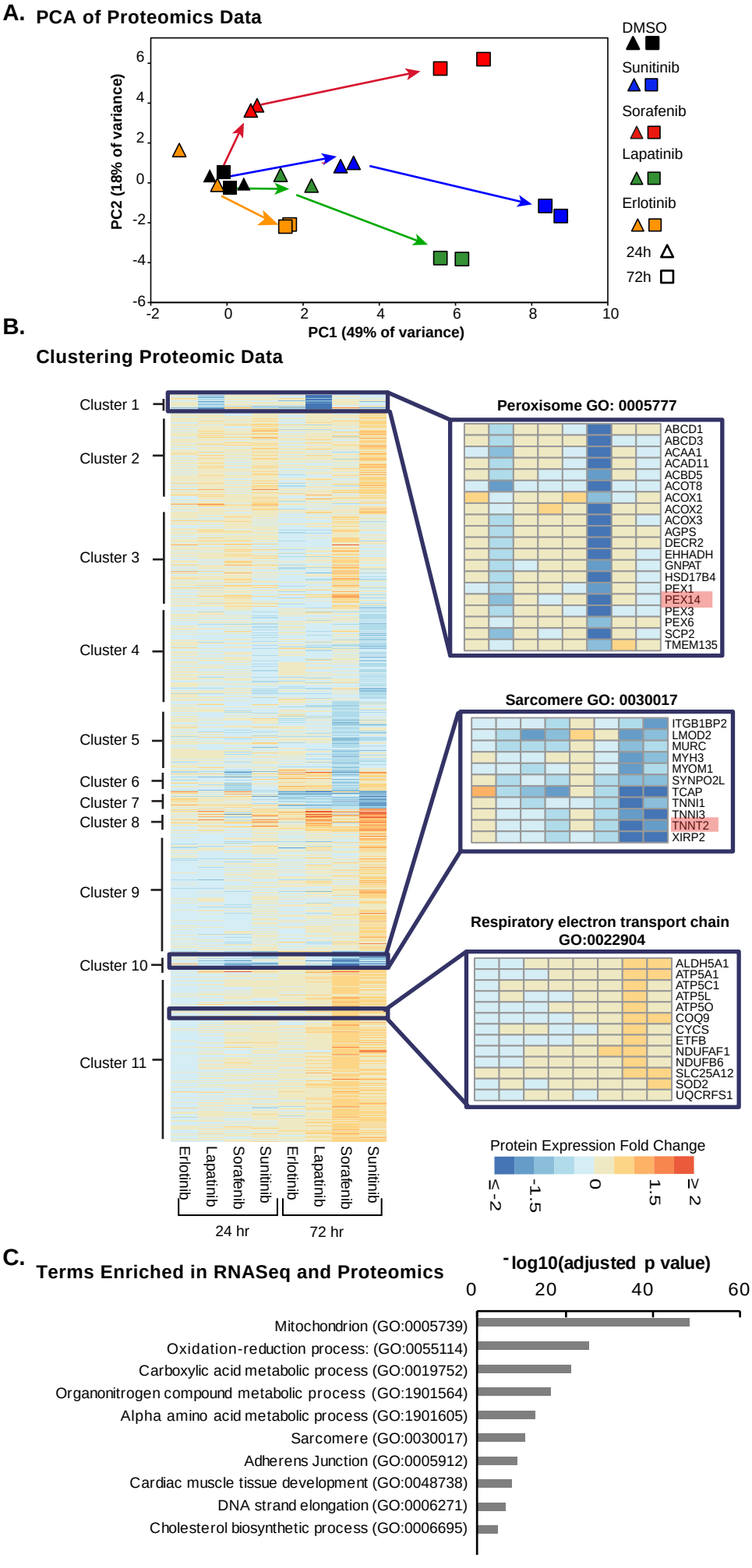

Figure 5

A. Staining for peroxisomes:

PEX14 Hoechst

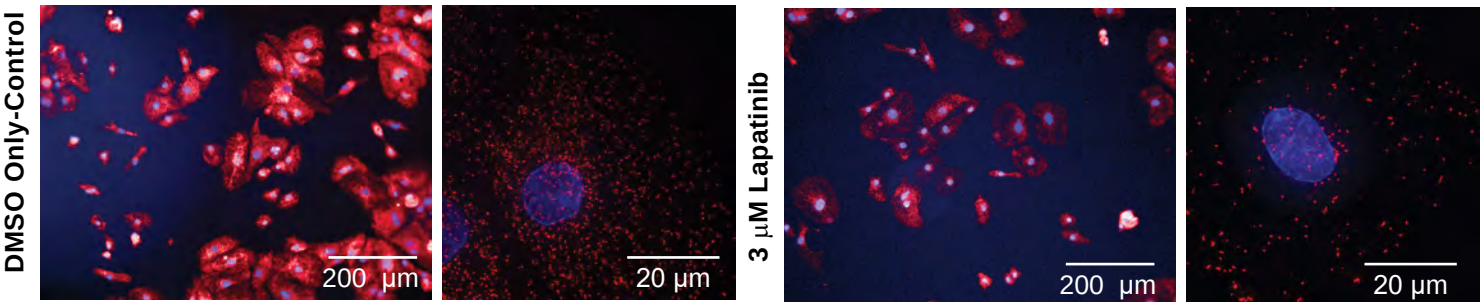

B. Staining cardiac isoforms of Troponin T

TNNT2 Hoechst

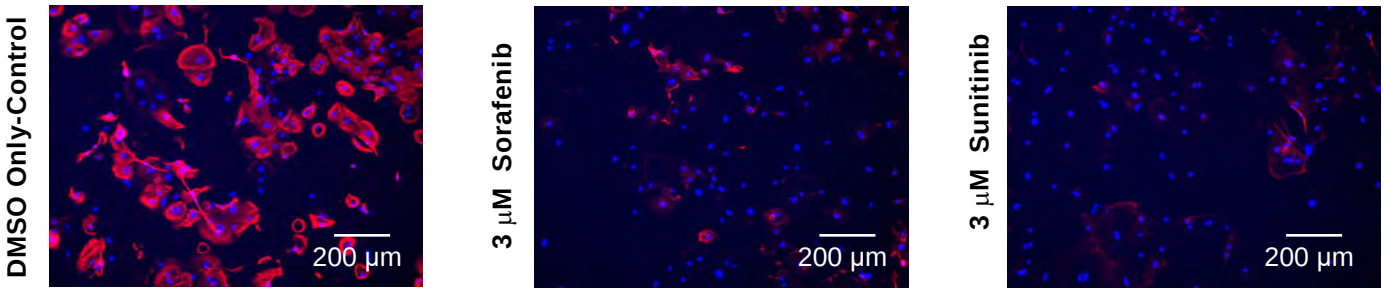

Figure 6

A. Experimental Design

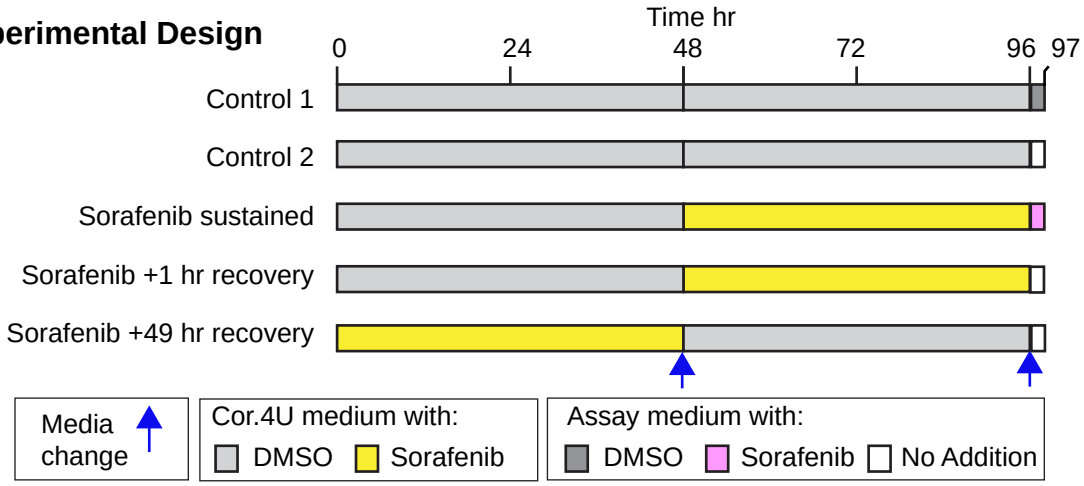

B. Oxygen Consumption Rate Assay

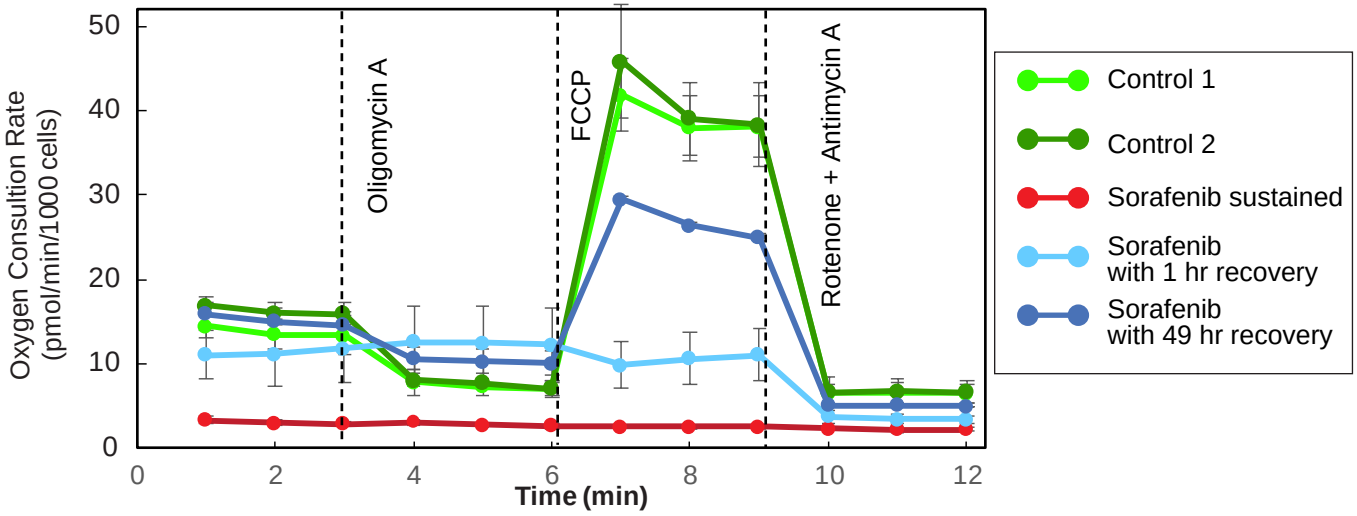

C. Metabolic Parameters

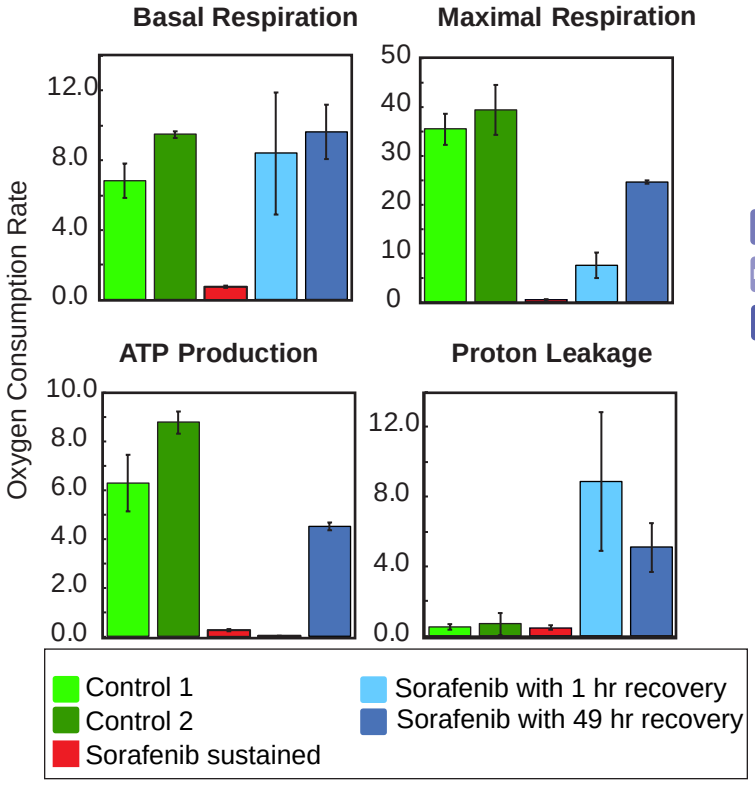

D. Downregulated Oxphos Genes

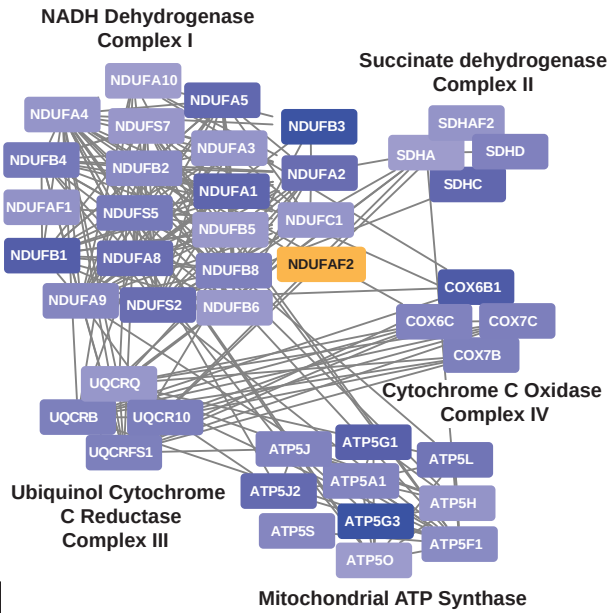

Figure 7

A. Media conditioning associated with glycolysis

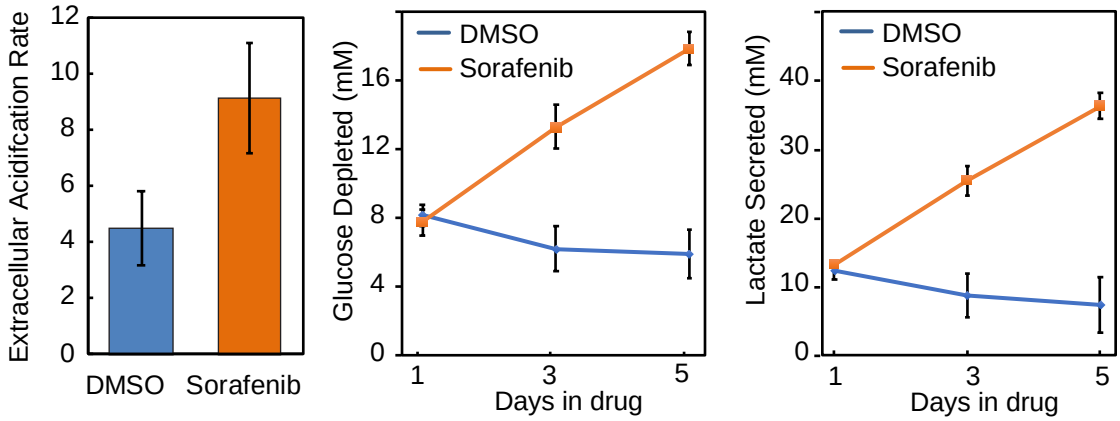

B. Co-drugging experimental design

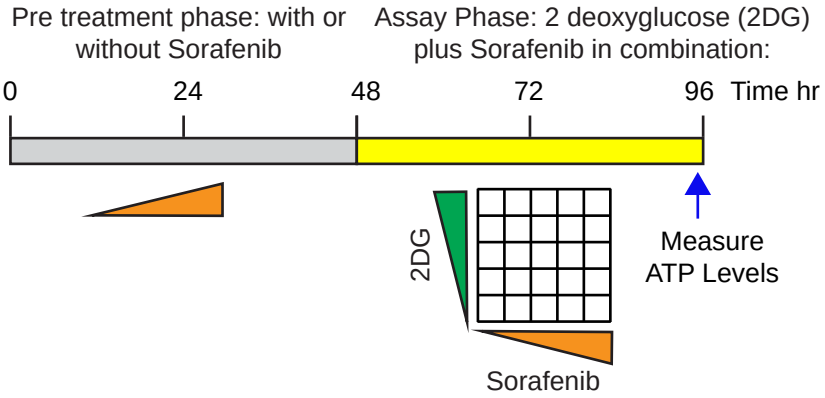

C. Impact of glycolytic shift on Sorafenib sensitivity